Metal–Support Interactions

International Edition: DOI: 10.1002/anie.201507821
German Edition: DOI: 10.1002/ange.201507821

Stabilization of Palladium Nanoparticles on Nanodiamond–Graphene Core–Shell Supports for CO Oxidation

*Liyun Zhang, Hongyang Liu, Xing Huang, Xueping Sun, Zheng Jiang, Robert Schlögl, and Dangsheng Su**

Abstract: *Nanodiamond–graphene core–shell materials have several unique properties compared with purely sp^2-bonded nanocarbons and perform remarkably well as metal-free catalysts. In this work, we report that palladium nanoparticles supported on nanodiamond–graphene core–shell materials (Pd/ND@G) exhibit superior catalytic activity in CO oxidation compared to Pd NPs supported on an sp^2-bonded onion-like carbon (Pd/OLC) material. Characterization revealed that the Pd NPs in Pd/ND@G have a special morphology with reduced crystallinity and are more stable towards sintering at high temperature than the Pd NPs in Pd/OLC. The electronic structure of Pd is changed in Pd/ND@G, resulting in weak CO chemisorption on the Pd NPs. Our work indicates that strong metal–support interactions can be achieved on a non-reducible support, as exemplified for nanocarbon, by carefully tuning the surface structure of the support, thus providing a good example for designing a high-performance nanostructured catalyst.*

The search for novel support materials with exceptional structures and properties that enhance the catalytic performance of metal nanoparticles (NPs) remains an important topic in heterogeneous catalysis.[1,2] Carbon materials, such as activated carbon, carbon nanotubes, and graphene, have been used as support materials.[3,4] Nanocarbon-supported metal catalysts show distinguished catalytic performances compared to catalysts supported on traditional carbon materials.[5,6] However, metal nanoparticles supported on these supports are unstable and tend to sinter to give larger species, especially under harsh reaction conditions. In our previous studies, a special form of nanocarbon, namely a nanodiamond–graphene core–shell material, was found to have unique properties and performed remarkably well as a metal-free catalyst.[7,8]

[*] L. Zhang, Dr. H. Liu, Prof. D. S. Su
Shenyang National Laboratory for Materials Science
Institute of Metal Research, Chinese Academy of Sciences
72 Wenhua Road, Shenyang 110016 (China)
E-mail: dssu@imr.ac.cn
Dr. X. Huang, Prof. R. Schlögl
Fritz Haber Institute of the Max Planck Society
Faradayweg 4–6, Berlin 14195 (Germany)
X. Sun, Prof. Z. Jiang
Shanghai Institute of Applied Physics
Shanghai Synchrotron Radiation Facility
Chinese Academy of Sciences
239 Zhangheng Road, Shanghai 201204 (China)

Supporting information for this article is available on the WWW under http://dx.doi.org/10.1002/anie.201507821.

In this work, a nanodiamond–graphene material comprising a nanodiamond core and a graphitic shell with just one or two graphene layers (ND@G) was carefully fabricated and used to support Pd NPs. We found that Pd NPs supported on the ND@G material exhibited superior catalytic activity in CO oxidation compared to Pd NPs supported on sp^2-bonded onion-like carbon (Pd/OLC). High-angle angular dark field scanning transmission electron microscopy (HAADF-STEM), Pd K-edge X-ray absorption spectroscopy, and temperature-programmed CO desorption (CO TPD) measurements were used to study the mechanism. The results show that the interaction between Pd and the support is stronger in Pd/ND@G than in Pd/OLC. This interaction affected the chemisorption properties of the Pd NPs, weakened the CO adsorption on Pd, and thus enhanced the catalytic activity of Pd/ND@G for CO oxidation.

A TEM image of the ND@G support is shown in Figure 1 a. The formation of a diamond core and a graphitic shell of one or two graphene layers is due to the graphitization of ND at 900 °C. Defects are indicated by white arrows in Figure 1 a and in the Supporting Information, Figure S1. When the ND materials were annealed at 1300 °C, an OLC structure with multiple graphitic shells was obtained, which,

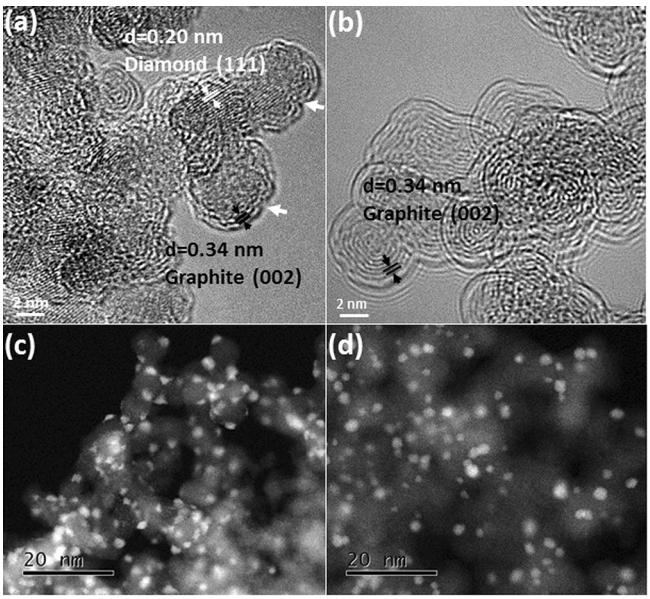

Figure 1. a, b) TEM images of the as-prepared nanocarbon supports: ND@G with a nanodiamond core and a defective graphene shell (a) and onion-like carbon (b). c, d) HAADF-STEM images of the corresponding nanocarbon-supported Pd catalysts: Pd/ND@G (c) and Pd/OLC (d).

however, still contained a small diamond core (Figure 1b). Raman spectra (Figure S3) also confirmed that the content of sp^2-hybridized carbon atoms of ND@G is much lower than that of OLC. The small ND core in the OLC is covered by a thick graphitic shell. Supported metal NPs will not interact with the ND core, so that the OLC can be considered as an sp^2-bonded nanocarbon support. Structural information on these two nanocarbon supports is summarized in Table 1. The

Table 1: Physicochemical properties of the nanocarbon materials.

Sample	S_{BET} [$m^2 g^{-1}$]	Pore volume [$cm^{-3} g^{-1}$]	O content[a] [at%]	C(sp^2)[a] [%]	I_D/I_G[b]
ND@G	342	1.51	2.4	40	0.72
OLC	358	1.56	0.9	71	0.58

[a] Determined by XPS. [b] Determined by Raman spectroscopy.

BET surface areas and pore volumes of the two nanocarbon materials do not show distinct differences. The oxygen contents are low, and the TPD spectra in Figure S2 show that most of the carboxylic acid, carboxylic anhydride, and lactone groups that could interact with metallic species were removed during high-temperature annealing;[9,10] it can thus be ruled out that oxygen functional groups play a role.

STEM images of the as-prepared Pd/ND@G and Pd/OLC catalysts (Figure 1c,d) show that the Pd NPs were uniformly dispersed on the ND@G and OLC supports. The average sizes of the Pd NPs on Pd/ND@G and Pd/OLC were about 1.9 nm and 2.2 nm, respectively (Figure S4; for additional TEM images, see Figures S5, S6). The Pd content of Pd/ND@G and Pd/OLC, which was determined by inductively coupled plasma mass spectrometry, was 2.38% and 2.30%, respectively.

The catalytic oxidation of CO as a probe reaction was evaluated over as-prepared Pd/ND@G and Pd/OLC samples in a temperature-programmed mode. The catalytic performance (Figure 2a) indicates that Pd NPs supported on ND@G are more active than those supported on OLC under reaction conditions with a stoichiometric amount of O_2 (1% CO, 0.5% O_2, He balance). 50% CO conversion (T_{50}) over the Pd/ND@G and Pd/OLC catalysts was achieved at 116°C and 146°C, respectively. The turnover frequency (TOF) of Pd/ND@G was about four times higher than that of the Pd/OLC catalyst (Figure 2b) at 50°C to 120°C. All of these findings indicate that the catalytic activity of the Pd/ND@G catalyst is superior to that of Pd/OLC.

We also carried out the CO oxidation under O_2-rich conditions (0.9% CO, 8.9% O_2, He balance). A substantially higher catalytic activity was observed for both catalysts compared to under O_2-stoichiometric reaction conditions. T_{50} over the Pd/ND@G and Pd/OLC catalysts was achieved at 70°C and 95°C, respectively (Figure S6a). The E_a value of Pd/ND@G for CO oxidation was also about 10 kJ mol^{-1} lower (Figure S7b), and the TOF was about three to four times higher than that of the Pd/OLC catalyst (Figure S7c), revealing the superiority of the Pd/ND@G sample in terms of CO oxidation. The Pd/ND@G catalyst also showed good stability over a 24 h reaction at 75°C (Figure S8a). When we

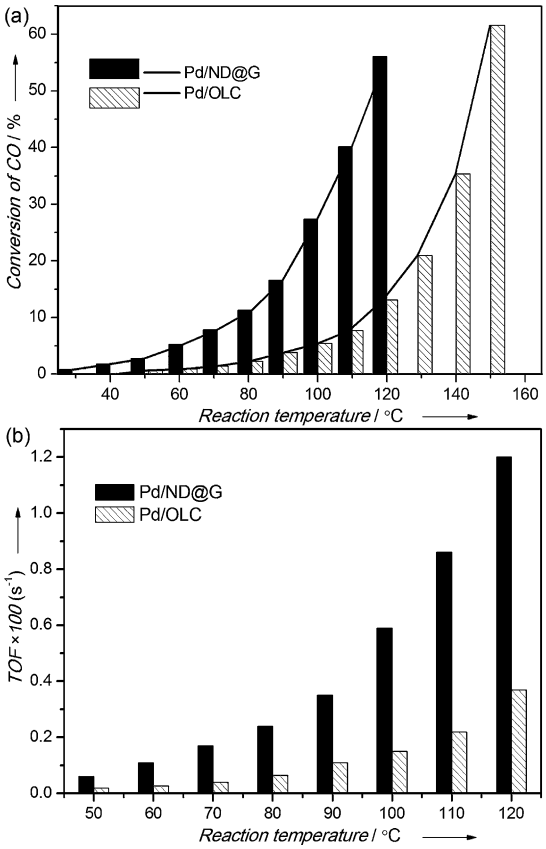

Figure 2. a) Temperature dependence of the CO oxidation reaction for the Pd/C catalysts. b) TOF versus temperature for Pd/ND@G and Pd/OLC samples ($CO/O_2 = 1:0.5$).

reused the Pd/ND@G catalyst, the T_{50} value increased slightly, but the activity could be easily recovered with H_2 reduction at 200°C (Figure S8b).

To understand the differences between Pd/ND@G and Pd/OLC, CO TPD experiments were carried out with samples of both catalysts. As shown in Figure 3, the curve of CO desorption is centered at around 90°C for Pd/ND@G, but at 121°C for the Pd/OLC sample. This indicates that CO

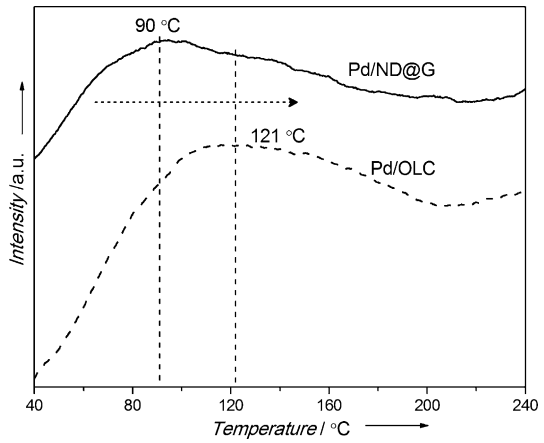

Figure 3. CO TPD spectra for Pd/ND@G and Pd/OLC.

adsorption on the Pd NPs is weakened in the Pd/ND@G system. Generally, for Pd catalysts, CO species adsorb strongly on the Pd surface in the low-temperature region, and the reaction rate is controlled by the desorption of CO.[11,12] The results of the CO TPD experiments suggest that the improvement of low-temperature CO oxidation over Pd/ND@G most likely results from the weakened CO chemisorption on the Pd NPs.

High-resolution HAADF-STEM images of the Pd/ND@G and Pd/OLC catalysts are shown in Figure 4. The morphologies and structures of the Pd NPs supported on

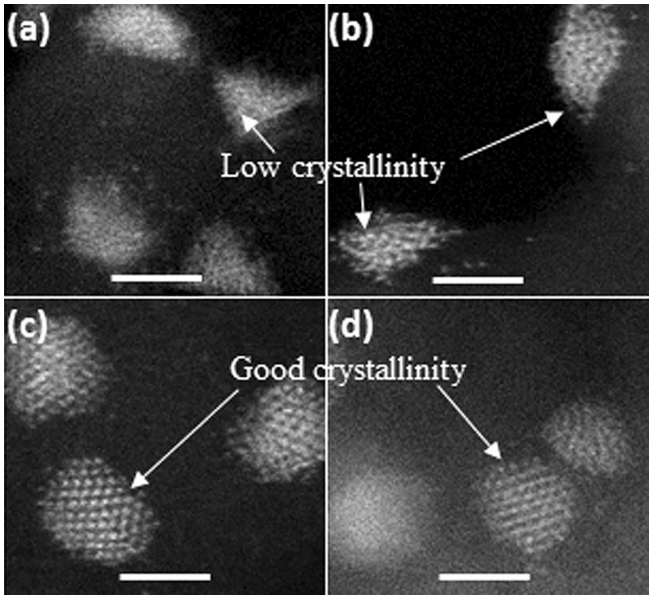

Figure 4. a–d) High-resolution HAADF-STEM images of Pd/ND@G (a, b) and Pd/OLC (c, d). Scale bars: 2 nm.

Nd@G and OLC are quite different. The Pd NPs in Pd/ND@G have more irregular (some triangular) shapes (Figure 1c and Figure 4a, b), whereas the Pd NPs in Pd/OLC exhibit a more round (or spherical) shape (Figure 1d and Figure 4c, d). The crystallinity of the supported Pd NPs in Pd/ND@G was much lower than that of the Pd NPs in Pd/OLC. Furthermore, the lattice fringes of the Pd NPs on the ND@G support are not as well resolved as those for Pd NPs on OLC. Considering these high-resolution HAADF-STEM images, we speculated that there might be a stronger metal–support interaction in Pd/ND@G, which contributes to the special morphology and the reduced crystallinity of the Pd NPs in Pd/ND@G. A stronger metal–support interaction in Pd/ND@G may also result in the formation of Pd–C bonds and thus lengthen the Pd–Pd bonds. Extended X-ray absorption fine structure (EXAFS) analysis (Table S3, Figure S10) revealed that the Pd–Pd bond lengths are 2.76 Å and 2.74 Å for Pd/ND@G and Pd/OLC, respectively. This trend is consistent with the above interpretation.

The sintering resistance of the supported Pd NPs was further investigated to understand the metal–support interactions in these two catalysts. The catalysts were annealed in Ar at 500 °C for 6 h. In the corresponding XRD pattern (Figure S13a) of the Pd/OLC sample, there is a sharp peak at 40.1°, which is due to the Pd(111) diffraction of the annealed Pd/OLC sample, indicating that the Pd NPs were sintered after being annealed at 500 °C. However, there is no obvious diffraction peak at 40.1° for the annealed Pd/ND@G sample, revealing that the Pd NPs in Pd/ND@G did not aggregate after annealing under the same conditions. The TEM images in Figure S12 show that the average size of the Pd NPs in Pd/ND@G slightly increased from 1.9 nm to 2.6 nm during annealing at 500 °C for 6 h, whereas in the Pd/OLC sample, it dramatically increased from 2.2 nm to 8 nm, which is in agreement with the XRD results. The high-temperature sintering resistance of Pd/ND@G further indicates that the metal–support interactions are stronger in Pd/ND@G than in Pd/OLC.

For metal–oxide support systems, the term "strong metal–support interactions" (SMSI) was first introduced to describe an electronic effect induced by metal–metal bonding,[13] causing a reduced sorption capacity of the metal particles. Later, the occurrence of SMSI in a system with reducible oxides was assigned to the migration of support species onto noble-metal particles, which decreases the accessible surface of the particles by encapsulation.[14–16] In our work, however, we did not observe obvious migration of carbon species from the support onto the Pd NPs and encapsulation of the NPs by STEM (Figure 4, S11b). DRIFT spectra of as-prepared and used catalysts upon CO adsorption also support that Pd NPs are not covered by carbon (Figure S11a). This is understandable as carbon is non-reducible. The improved CO oxidation over Pd/ND@G compared to that over Pd/OLC indicates that for a non-reducible system, at least for carbon, a reduction in the sorption capacity could be achieved by simply changing the support structure while keeping the composition the same. Strong metal–carbon interactions with the formation of Pd–C bonds may lead to a charge redistribution on Pd and thus weaken the chemisorption of CO. The strong interaction between Pd and the carbon support may also hinder the relaxing of Pd to form particles with well-ordered crystallinity and extended surfaces (as revealed by the high-resolution HAADF-STEM images in Figure 4). Pd nanoparticles with more low-coordination sites on the ND support have reduced sorption capacities as CO interacts more strongly with extended surfaces with bridge or threefold hollow sites.[17] Furthermore, Pd particles with less relaxed structures can more efficiently dissociate O_2 than Pd with extended surfaces, which may further improve the CO oxidation reaction. DFT calculations on model systems consisting of a defective graphene sheet and metal clusters predict a strong support–metal interaction.[18,19] The high-resolution (S)TEM images reveal that the one or two graphene layers of ND@G could be somehow more defective than the surface layer of OLC, but the strong interaction between Pd and NG could also be modified by the sp^3-bonded diamond core, owing to the similar lattice types of diamond and Pd,[20] but this hypothesis needs to be further explored.

In conclusion, a nanodiamond–graphene material composed of a nanodiamond core and a defective graphitic shell (ND@G) and an OLC support as a control sample have been prepared. When Pd NPs are supported on ND@G, they

displayed superior CO oxidation activity and high-temperature sintering resistance compared to Pd NPs on the OLC support. There may be Pd–C bond formation in Pd/ND@G, which may induce changes in the Pd electronic structure and weaken the CO adsorption on the Pd surface, resulting in the distinct improvement of the catalytic performance of the Pd/ND@G catalyst in CO oxidation compared to the Pd/OLC catalyst. Furthermore, the special morphologies, the reduced crystallinity, and the improved sintering resistance of the Pd NPs in ND@G indicate that there is a stronger metal–support interaction in Pd/ND@G than in Pd/OLC, which may also result from the formation of Pd–C bonds. The superior performance as well as the strong metal–support interactions in Pd/ND@G may be affected by both the sp^3-bonded ND core and the sp^2-bonded defective graphitic shell. Our work indicates that strong metal–support interactions can be achieved on a non-reducible support, as exemplified for nanocarbon, by carefully tuning the surface structure of the support. This approach may offer a direction to fabricate novel support materials for high-performance carbon-supported catalysts.

Experimental Section

Supported Pd catalysts were prepared by the deposition–precipitation method. CO TPD data were obtained by using a homemade TPD apparatus. First, a sample (100 mg) was treated at 200 °C for 1 h in 10 % H_2 atmosphere. Second, the adsorption of CO molecules was conducted at 35 °C for 120 min to guarantee the saturated adsorption of CO on the Pd surface. The heating rate was 2 K min^{-1}. CO oxidation was carried out at ambient pressure in a temperature-programmed mode with a rate of 1 K min^{-1}. Two different CO oxidation rates were obtained, in 1 % CO and 0.5 % O_2 with a balance of He and in 0.9 % CO and 8.9 % O_2 with a balance of He, respectively.

Acknowledgements

We acknowledge financial support from MOST (2011CBA00504), the NSFC of China (21573254, 21203214, 21133010, 51221264, and 21261160487), the Youth Innovation Promotion Association (CAS), and the "Strategic Priority Research Program" of the Chinese Academy of Sciences (XDA09030103).

Keywords: CO oxidation · graphene · metal–support interactions · nanodiamonds · palladium nanoparticles

How to cite: *Angew. Chem. Int. Ed.* **2015**, *54*, 15823–15826
Angew. Chem. **2015**, *127*, 16049–16052

[1] R. T. K. Baker, E. B. Prestridge, R. T. Garten, *J. Catal.* **1979**, *59*, 293–302; V. M. Gonzalez-DelaCruz, J. P. Holgado, R. Pereñíguez, A. Caballero, *J. Catal.* **2008**, *257*, 307–314; L. Shao, B. Zhang, W. Zhang, S. Y. Hong, R. Schlögl, D. S. Su, *Angew. Chem. Int. Ed.* **2013**, *52*, 2114–2117; *Angew. Chem.* **2013**, *125*, 2168–2171.
[2] A. Fihri, M. Bouhrara, U. Patil, D. Cha, Y. Saih, V. Polshettiwar, *ACS Catal.* **2012**, *2*, 1425–1431; A. Lilly Thankamony et al., *Angew. Chem. Int. Ed.* **2015**, *54*, 2190–2193; *Angew. Chem.* **2015**, *127*, 2218–2221.
[3] P. Serp, M. Corrias, P. Kalck, *Appl. Catal. A* **2003**, *253*, 337–358.
[4] D. S. Su, S. Perathoner, G. Centi, *Chem. Rev.* **2013**, *113*, 5782–5816.
[5] E. Yoo, T. Okata, T. Akita, M. Kohyama, J. Nakamura, I. Honma, *Nano Lett.* **2009**, *9*, 2255–2259; A. Villa, D. Wang, N. Dimitratos, D. S. Su, V. Trevisan, L. Prati, *Catal. Today* **2010**, *150*, 8–15.
[6] R. S. Oosthuizen, V. O. Nyamori, *Platinum Met. Rev.* **2011**, *55*, 154–169; H. Liu, J. Wang, Z. Feng, Y. Lin, D. S. Su, *Small* **2015**, *11*, 5059–5064.
[7] R. Wang, X. Sun, B. Zhang, X. Sun, D. S. Su, *Chem. Eur. J.* **2014**, *20*, 6324–6331.
[8] X. Liu, B. Frank, W. Zhang, T. P. Cotter, R. Schlögl, D. S. Su, *Angew. Chem. Int. Ed.* **2011**, *50*, 3318–3322; *Angew. Chem.* **2011**, *123*, 3376–3380.
[9] B. F. Machado, M. Oubenali, M. R. Axet, T. T. NGuyen, M. Tunckol, M. Girleanu, O. Ersen, I. C. Gerber, P. Serp, *J. Catal.* **2014**, *309*, 185–198.
[10] L. Zhang, G. Wen, H. Liu, N. Wang, D. S. Su, *ChemCatChem* **2014**, *6*, 2600–2606.
[11] H. J. Freund, G. Meijer, M. Scheffler, R. Schlögl, M. Wolf, *Angew. Chem. Int. Ed.* **2011**, *50*, 10064–10094; *Angew. Chem.* **2011**, *123*, 10242–10275.
[12] P. J. Berlowitz, C. H. F. Peden, D. W. Goodman, *J. Phys. Chem.* **1988**, *92*, 5213–5221.
[13] S. J. Tauster, S. C. Feng, R. L. Garten, *J. Am. Chem. Soc.* **1978**, *100*, 170.
[14] R. T. Baker, E. B. Frestirigde, R. L. Garten, *J. Catal.* **1979**, *56*, 390–406; J. Santos, J. Philips, J. A. Dumisic, *J. Catal.* **1983**, *81*, 147–167.
[15] D. J. Dwyer, J. L. Robbins, S. D. Cameron, N. Dudash, J. Hardenberg in *Strong Metal-Support Interaction* (Eds.: R. T. K. Baker, S. J. Tauster, J. A. Dumesic), ACS Symposium Series, Washington, **1986**, p. 21.
[16] R. Naumann d'Alnoncourt, M. Freidrich, E. Kunkes, D. Rosentahl, F. Giegsdies, B. Zhang, L. Shao, M. Schuster, M. Behrens, R. Schloegl, *J. Catal.* **2014**, *317*, 220–228.
[17] A. F. Carlsson, M. Naschitzki, M. Bäumer, H. J. Freund, *J. Phys. Chem. B* **2003**, *107*, 778–785.
[18] M. Zhou, A. Zhang, Z. Dai, C. Zhang, Y. P. Feng, *J. Chem. Phys.* **2010**, *132*, 194704.
[19] Y. Okamoto, *Chem. Phys. Lett.* **2006**, *420*, 382–386.
[20] N. N. Vershinin, O. N. Efimov, V. A. Bakaev, A. E. Aleksenskii, M. V. Baidakova, A. A. Sitnikova, A. Y. Vul, *Fullerenes Nanotubes Carbon Nanostruct.* **2011**, *19*, 63–68.

Received: August 21, 2015
Published online: November 16, 2015

